

Article

Growth of GaN Thin Film on Amorphous Glass Substrate by Direct-Current Pulse Sputtering Deposition Technique

Wei-Sheng Liu * , Yu-Lin Chang and Hui-Yu Chen

Department of Electrical Engineering, Yuan Ze University, Chung-Li 32003, Taiwan

* Correspondence: wsliau@saturn.yzu.edu.tw

Received: 27 May 2019; Accepted: 27 June 2019; Published: 30 June 2019



Abstract: We deposited 300-nm-thick GaN films on an amorphous glass substrate at a substrate temperature of 300 °C by using pulsed direct current (DC) sputtering. A ZnO buffer layer was utilized to improve the crystalline quality of the GaN films. Scanning electron microscopy results showed that the GaN thin films were grown along the *c*-axis and possessed a columnar structure. Atomic force microscopy results revealed that the GaN film deposited at a sputtering power of 75 W had the maximum grain size (24.1 nm). Room-temperature photoluminescence measurement of the GaN films indicated an ultraviolet near-band-edge emission at 365 nm and a Zn impurity energy transition level at 430 nm. In addition, X-ray diffraction conducted on the GaN films revealed a predominant (002) hexagonal wurtzite structure. The GaN film deposited at the sputtering power of 75 W demonstrated a high optical transmittance level of 88.5% in the wavelength range of 400–1100 nm. The material characteristics of the GaN films and ZnO buffer layer were studied using cross-sectional high-resolution transmission electron microscopy. The deposition of GaN films by using pulsed DC magnetron sputtering can result in high material quality and has high potential for realizing GaN-related optoelectronic devices on glass substrates.

Keywords: gallium nitride; photoluminescence; DC-pulse magnetron sputtering; zinc oxide; buffer layer; transmission electron microscopy

1. Introduction

Gallium nitride (GaN) films have a wide energy band gap along with inherent advantages of chemical and thermal stability, hardness, high thermal conductivity, high breakdown voltage, and electron mobility [1]. Such films have high potential for application in high-quality optoelectronic devices such as light-emitting diodes; in addition, they can be applied in other electronic devices such as field-effect transistors, heterojunction bipolar transistors, and high-electron mobility transistors [2,3]. For high-temperature operations and high-power electronic applications, GaN films and their related compound materials are relatively favorable because of their wide energy band gap and excellent thermal stability. In addition to the particularly high energy band gap of GaN films, the flexibility of the tunable energy band alignment for the nitride-related heterostructure in a GaN matrix is indispensable in developing a variety of optoelectronic devices [4] by using aluminum nitride (6.2 eV) and indium nitride (1.9 eV) compound materials for the wide modulation of the energy band alignment of GaN-related compound materials.

Presently, several thin film deposition techniques, such as metalorganic chemical vapor deposition [5], molecular beam deposition [6], and hydride vapor phase epitaxy [7], are widely used in industry and academia for growing high-quality GaN thin films on sapphire (Al₂O₃) or monocrystalline silicon substrates. Although a large lattice mismatch of 15% exists between a sapphire substrate and a GaN

film [1], the crystal dislocation that is typically induced by the lattice mismatch can be minimized by utilizing a buffer layer and patterned sapphire. Sapphire substrates are still the most common substrates for growing high-quality GaN films [8].

However, to develop large-area GaN-related devices on low-cost glass or flexible plastic substrates such as Polyimide (PI), Polyethylene Terephthalate (PET), Polyethylene Naphthalate (PEN), and Polyether sulfone (PES), the GaN films and their related compound layers should be grown at a low substrate temperature to prevent the melt of the glass or flexible plastic substrates. Therefore, developing a low-temperature deposition technology for growing GaN films on glass substrates is essential. According to the literature, GaN films can be deposited using magnetron sputtering on glass substrates, and this process involves the following advantages: Increased thin film deposition rate, large-area and low-temperature deposition, and reduced harmful byproducts during GaN film fabrication [9,10].

The crystal quality of GaN films grown on glass substrates is in terms of the thin film deposition rate, growth temperature, and buffer layer insertion between the film and glass substrate. Radio frequency (RF) plasma magnetron sputtering has been reported to be a suitable technique for growing GaN films on glass substrates because the sputtering power can be easily modulated to enhance the kinetic energy of adatoms, consequently engendering adatom migration and thin film growth [11]. Although GaN films can be grown on glass substrates through RF sputtering, the thin film deposition rate and crystal quality of GaN films can be further improved.

In recent years, pulsed direct current (DC) magnetron sputtering has been regarded as a novel deposition technique because it exhibits a thin film deposition rate higher than that achieved using the conventional RF magnetron sputtering system [12]. It has a wide adjustment range for the pulse frequency (5–350 kHz), and the pulse frequency can be easily adjusted to reduce the arc discharge generated during the sputtering process. In previous research, the arc generated by pulsed DC magnetron sputtering was reduced because the charge accumulated on the target surface during pulse polarity modulation was eliminated. The corresponding mechanism was reported to involve the conversion of the target voltage to a positive voltage to eliminate the accumulated positive charges; thus, fewer arc events were observed on using pulsed DC magnetron sputtering [13].

According to previous reports, pulsed DC sputtering can result in a high thin film quality. Furthermore, the DC pulse frequency is closely related to the thin film quality. A study reported that the defect density in thin films decreased considerably as the frequency of pulsed DC sputtering increased [14]. Pulsed DC sputtering enables films to have dense nucleation sites along with a high thin film growth rate and high crystalline quality. Moreover, the irregularity in the shape and size of a crystallite, caused by the arc event during sputtering, has been reported to be considerably reduced [12,15,16]. Therefore, pulsed DC sputtering engenders a relatively smooth film surface. The DC pulse power supply can also solve problems such as plasma instability, arc discharge, and target poisoning during metal oxide deposition [17].

In this study, we successfully deposited GaN films on a glass substrate by using pulsed DC sputtering at a low growth temperature. To realize a high-quality GaN film, a zinc oxide (ZnO) layer was used as a buffer layer and inserted between the GaN film and amorphous glass substrate since high crystal quality of the ZnO layer was easily grown on glass substrate through sputtering-deposition method, meanwhile, there existed a low lattice mismatch of 2.2% [18] between the ZnO and GaN layer. The study results indicated that pulsed DC sputtering has high potential for realizing the growth of a high-quality GaN film on a large-area amorphous glass substrate for optoelectronic devices, thereby realizing a low fabrication cost.

2. Materials and Methods

In this study, GaN films were grown on Corning E2K glass substrates, with a ZnO layer serving as the buffer layer. The ZnO buffer layer was first grown using RF magnetron sputtering with a 3-inch ZnO target (purity: 99.99%). After the deposition of the ZnO buffer layer, the GaN film was

subsequently grown using pulsed DC magnetron sputtering with a 3-inch GaN target (purity: 99.99%). Prior to thin film deposition, the sputtering chamber was evacuated using a high vacuum pressure of approximately 5.33×10^{-4} Pa; the processing pressure was 1.33×10^{-1} Pa for ZnO buffer layer and 1.99 Pa for GaN film growth using argon (Ar) gas flow rates of 30 and 15 sccm, respectively. Both targets were pre-sputtered 1 min for cleaning the target surface. The argon: nitrogen gas mixing ratio was set at 1:1 for GaN film deposition, whereas pure Ar process gas (30 sccm) was used for the growth of the ZnO buffer layer. The distance between the target and the substrate was 15 cm and the thin-film deposition rates were 0.14 nm/s for ZnO buffer layer and 0.18, 0.14 and 0.11 nm/s for GaN thin-film growth with sputtering powers of 125, 100 and 75 W, respectively. A 100-nm-thick ZnO buffer layer was grown using an RF sputtering power of 150 W at a substrate temperature of 300 °C, followed by post in situ annealing at 400 °C with annealing time of 100 s in a vacuum environment. A 300-nm-thick GaN film was subsequently grown at a substrate temperature of 300 °C using pulsed DC sputtering at varied sputtering powers of 75, 100, and 125 W.

The crystallite structural properties of the films were analyzed through X-ray diffraction (XRD) using a Cu-K α ($\lambda = 1.54052 \text{ \AA}$) irradiation source in a grazing incidence XRD configuration that involved 2θ scan angles of 10° – 80° . The lattice structure of the ZnO buffer layer and GaN films were studied using a transmission electron microscopy (TEM) system. A selected area electron diffraction (SAED) system equipped on the TEM system (JEM2100) was used to analyze SAED lattice diffraction patterns and high-resolution lattice images. The operational voltage was 200 KV for both the TEM and SAED processes, with the magnification factors being 600,000 \times and 100 \times , respectively. Elemental analyses for the ZnO buffer layer and GaN films were conducted using a secondary ion mass spectroscopy (SIMS) measurement. Photoluminescence (PL) measurements were conducted using a 30-mW He-Cd laser excitation at a wavelength of 325 nm at 10 K and room temperature. The optical transmittance of the GaN samples examined in this study was determined using an ultraviolet-visible spectrophotometer with reference to a glass substrate over an optical wavelength range of 300–1100 nm.

3. Results and Discussions

In this study, all GaN films demonstrated crystal growth on glass substrates. The XRD image of the GaN films shown in Figure 1a,b illustrates the XRD patterns of the ZnO buffer layer and GaN films, respectively, grown at various pulsed DC sputtering powers from 75 to 125 W. The ZnO buffer layer was grown using an RF magnetron sputtering power of 150 W. The peak was along the c-axis (002) hexagonal wurtzite structure—with the predominant XRD peak being observed at a 2θ angle of approximately 34.4° —and had a narrow full width at half maximum (FWHM) value of 0.542° , indicating the superior quality of the ZnO buffer layer grown on the glass substrate.

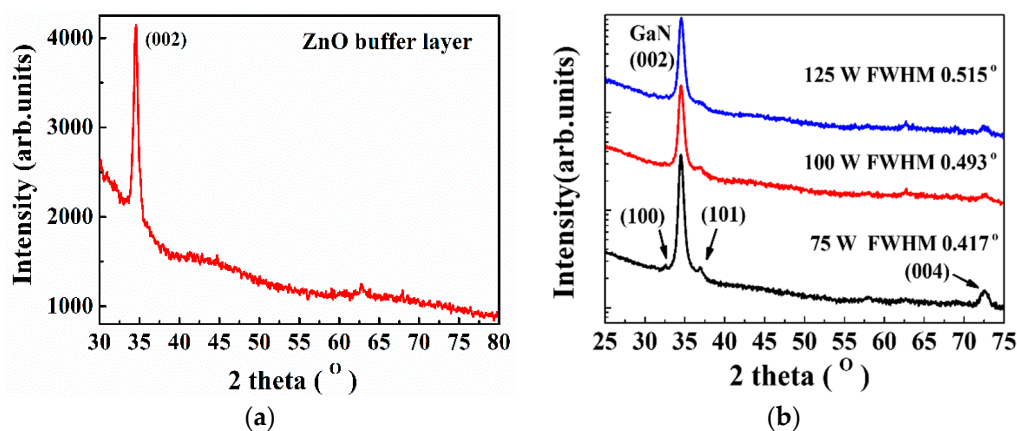


Figure 1. (a) X-ray diffraction (XRD) patterns of ZnO, and (b) the XRD patterns of GaN films deposited on ZnO/Glass with sputtering powers of 75, 100 and 125 W. All the GaN films exhibited the (002) hexagonal wurtzite structure.

The GaN films deposited on an amorphous glass substrate in this study demonstrated clear and narrow XRD FWHM values because of the superior crystal quality and optimal structural properties provided by the ZnO buffer layer, which contributed to the grain growth of the GaN films [19]. Additionally, during the sputtering process, a mixed process gas of Ar and N₂ was excited through electrical discharge to form Ar⁺ and N⁺ plasma ions, which were accelerated by a negative bias applied to the substrate. Thus, the amount of plasma ions and degree of ion bombardment were affected. These factors can considerably affect the compositions, structures, and morphological properties of GaN films [20]. Consequently, the introduction of the ZnO buffer layer and the appropriate Ar:N₂ mixing ratio in this study contributed to the superior crystal quality of the GaN films possessing high XRD intensity and narrow XRD FWHM values.

As presented in Figure 1b, the XRD spectra revealed the presence of peaks at 2θ angles of 32.5°, 34.5°, 36.9°, and 72.6°, which were determined to correspond to the (100), (002), (101), and (004) crystal orientations of the GaN films, respectively [21]. Accordingly, the spectra revealed that for all GaN samples, the (002) hexagonal wurtzite structure had a predominant XRD peak position at the 2θ angle of approximately 34.5°. This *c*-axis orientation was considered to result from the lowest surface energy of the (002) lattice plane in the GaN films, leading to preferential growth in the (002) direction. In addition, XRD peaks at 2θ angles of the 32.5° and 36.9°, corresponding to typical hexagonal wurtzite GaN of (100), (101) lattice planes, respectively, according to JCPDS card No.65-3410. The 2θ angle discrepancy of the XRD (100), and (101) peaks presented a small shift compared with the theoretical values, which indicated the tensile stress caused by the lattice mismatch between the GaN film and the glass substrate [22,23].

The XRD FWHM values also decreased significantly from 0.515° to 0.417° as the sputtering deposition power decreased from 125 to 75 W. The GaN film deposited at the low sputtering power of 75 W displayed superior XRD intensity with a narrow FWHM value of 0.417°. The XRD FWHM value is a vital parameter for assessing the average crystallite size according to the Scherrer formula [24,25]:

$$D = \frac{0.9\lambda}{\beta \cos \theta} \quad (1)$$

where *D* is the grain size, λ is the X-ray wavelength (0.154 nm), β is the XRD (002) FWHM, and θ is the Bragg angle. The grain sizes calculated from the Scherrer formula are 23.1, 19.5, and 18.7 nm for the GaN films with the standard deviations of the FWHM as 0.079, 0.087, and 0.091 for GaN with sputtering powers of 75, 100 and 125 W, respectively, which are agreed with the atomic force microscopy (AFM) measurement results. As revealed by XRD analyses, the sputtering deposition of the GaN film with the ZnO buffer layer by using a low sputtering power of 75 W demonstrated a narrow FWHM value of 0.417°, indicating that the GaN film grown on the glass substrate was of superior quality.

The high-resolution TEM (HRTEM) images and SAED patterns of the ZnO and GaN films are depicted in Figure 2; the cross-sectional image of GaN/ZnO combination layers on the glass substrate is depicted in Figure 2a, and the magnified lattice images for the ZnO and GaN films are displayed in Figure 2b. Because of the large lattice mismatch (15%), an obvious threading dislocation is expected in a single-crystal GaN film grown on a sapphire substrate through metalorganic chemical vapor deposition [5]. However, in this study, the GaN film with a polycrystalline structure that was grown along *c*-axis direction on the ZnO buffer layer by using pulsed DC sputtering (Figure 2a), and the threading dislocation density was calculated as 1.72 × 10¹¹ cm⁻², which was slightly higher than those of grown on sapphire substrates by using MOCVD technology (approximately 10⁸ to 10¹⁰ cm⁻²) [26].

The interface image of ZnO and GaN films were clearly shown by the HRTEM measurement in Figure 2b, the nanoisland structures with different orientations revealed that the GaN film exhibited a polycrystalline structure, where the lattice arrangement is nearly regular corresponding to the narrow XRD FWHM value in Figure 1b and the preceding analysis demonstrates that the results of this study are rather satisfactory, and the GaN film grown on the glass substrate exhibited a high-quality crystal growth. The SAED patterns observed for the GaN thin film (Figure 2c) revealed a diffraction ring,

signifying polycrystalline structures. As illustrated in the SAED patterns of the GaN film (Figure 2c), we can observe that diffraction spots are superposed on the amorphous halo indicating the hexagonal wurtzite structure with (100), (002) and (101) crystal planes marked on the Figure 2c, demonstrating that the GaN film had a well-ordered SAED pattern of polycrystalline orientation spots possessing advanced thin film quality [27,28]. The interplanar spacing (d_{hkl}) values of 2.41, 2.56 and 2.77 Å were calculated, which corresponded to the GaN (100), (002), and (101) planes, respectively [29].

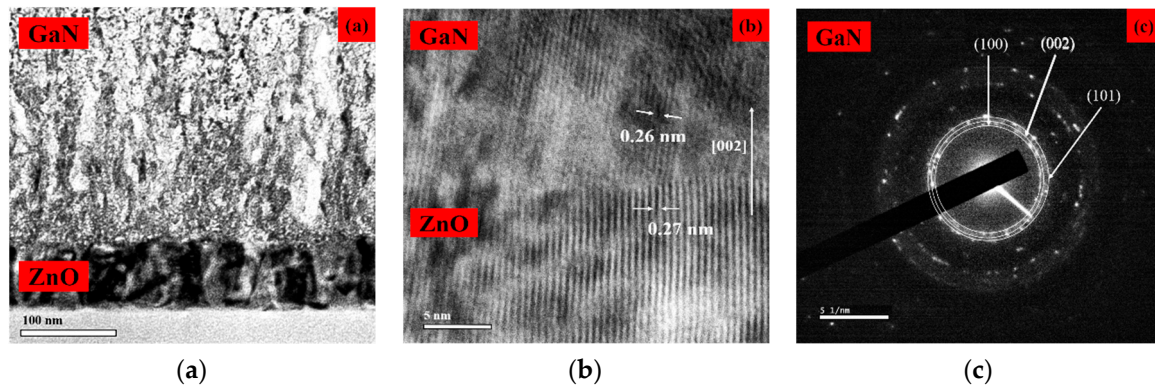


Figure 2. High-resolution TEM (HRTEM) images and selected area electron diffraction (SAED) diffraction patterns of ZnO and GaN films: (a) The cross-sectional image of GaN/ZnO combination layers on glass substrate; (b) The lattice images for GaN films; (c) and the SAED patterns for GaN films.

Additionally, the SIMS analysis were performed in order to confirm the elemental composition in all samples for chemical compositional study of GaN film with sputtering power of 75 W in Figure 3. From the SIMS results, the elements of gallium, nitrogen, zinc, oxygen, carbon were found in the GaN film. Additionally, an obvious Zn diffusion from ZnO buffer layer to GaN layer was clearly observed in the SIMS measurement.

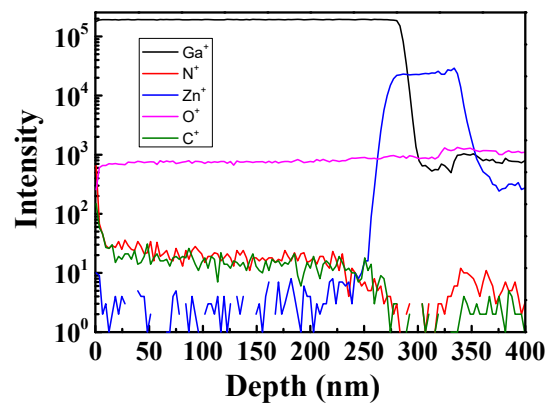


Figure 3. Secondary Ion Mass Spectroscopy (SIMS) measurement of GaN film with ZnO buffer layer grown on the amorphous glass substrate.

According to atomic force microscopy (AFM) observation results for the GaN samples (Figure 4), the grain sizes were estimated to be 24.1, 22.6, and 21.7 nm with the standard deviations of the grain size as 1.37, 2.08, and 2.54 for the sputtering powers of 75, 100, and 125 W, respectively. During the process of thin film deposition at a low sputtering power, despite the low deposition rate, the low sputtering power considerably contributed to the formation of relatively large grain sizes. By contrast, at a high sputtering power, the sputtering particulates could have excess kinetic energy, leading to a very high deposition rate and consequently the formation of smaller grain sizes, thereby degrading the thin film crystal quality [30,31]. According to previous studies, the deposition rate of high-power sputtering and the increase in high-energy ion bombardment can engender damage to the GaN thin

film surface and thus reduce the surface diffusion of adatoms, thereby impeding crystallite formation. Thus, using a relatively low and appropriate sputtering power can ensure the effective nucleation growth of crystals leading to superior GaN thin film quality.

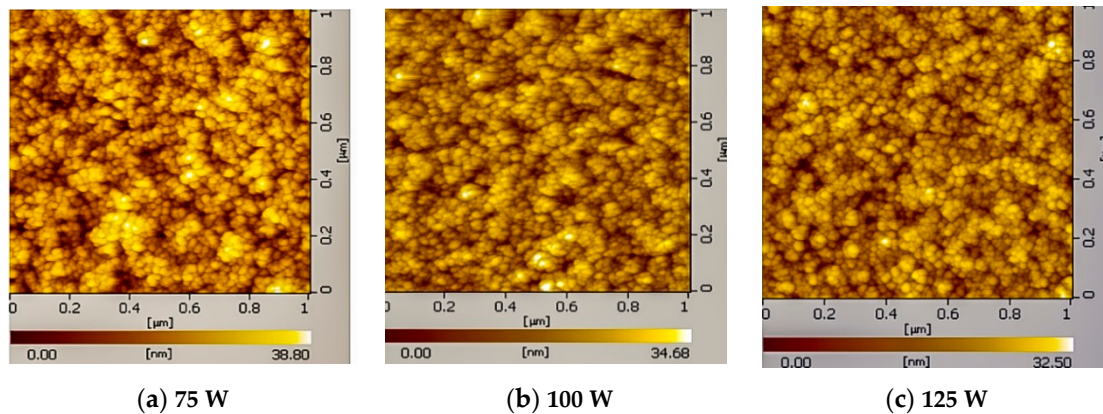


Figure 4. 2D AFM surface roughness images of GaN thin films deposited by DC-pulse sputtering at different powers of 75 W (a), 100 W (b), and 125 W (c), the grain size values were 24.1 (a), 22.6 (b), and 21.7 nm (c), respectively.

To understand the material characteristics of GaN films, PL measurements were performed in this study. A 325-nm (3.8 eV) laser excitation source, with a laser photon energy level higher than the energy band gap of GaN films (3.4 eV), was used to investigate the optical properties of the GaN films. Through the PL measurements, the energy band gap, impurity type, carrier energy transition behavior, stoichiometry or material composition distribution, crystal quality, and defect type in the GaN films could be comprehensively studied [32,33]. To develop high-quality GaN films through sputtering deposition on a glass substrate and to realize a near-band-edge (NBE) luminescence emission at 365 nm, investigating the carrier energy transition through the defect and donor/acceptor states is critical [34,35].

The largest grain size was observed in the GaN film deposited at a sputtering power of 75 W, and the corresponding PL spectra are presented in Figure 5; the room-temperature (300 K) and low-temperature (10 K) PL measurement results are shown in Figure 5a,b, respectively. The PL spectral emission peak was observed at 430 nm (2.88 eV), with a spectral shoulder appearing at 365 nm (3.4 eV). The peak position at 365 nm was determined to correspond to an NBE emission in GaN thin films with a hexagonal crystal structure. The peak position from 413 to 460 nm (3.0–2.7 eV; the peak was obvious at 2.88 eV in this study) show in Figure 5b, was determined to represent the blue luminescence (BL) band in GaN thin films [36]. The peak position at 430 nm in the BL band was observed to indicate a deep defect level of undoped GaN films, and this peak was considered as an energy transition from the conduction band or shallow donor level to the deep acceptor energy level, which was associated with zinc impurities observed in GaN films [37,38].

In this study, the ZnO layer was used as the buffer layer for GaN film growth at a substrate temperature of 300 °C. The Zn element might diffuse from the buffer layer to the GaN film, which was observed by the SIMS measurement, during the sputtering process. Therefore, the PL emission peak at 430 nm could be explained in terms of Zn impurity energy level in GaN films [19]. Figure 5b illustrates the low-temperature PL measurements for the GaN film deposited at a sputtering power of 75 W. The PL spectrum shows the fingerprints in unintentionally doped GaN films, indicating a fine crystal structure. In addition to the NBE emission observation at 365 nm, typical defects were clearly observed at the 413 and 540 nm emission peaks. The spectral peak position at 413 nm (3.0 eV) might have resulted from the carrier transition from the C_{Ga} donor level to the C_N acceptor level (the presence of carbon impurities can be clearly observed in SIMS measurement), which was verified through the calculation results obtained through density functional theory [39,40]. Moreover, the

GaN film PL spectrum of the yellow luminescence (YL) band (2.3 to 2.1 eV) is shown in Figure 5b. In this study, the YL band of GaN exhibited a peak at 540 nm (2.3 eV), which can be ascribed to the Ga vacancies (V_{Ga}) point defects [41,42]. For carrier recombination through defect states in undoped GaN films, considerable research has been conducted on the origin of YL emissions, and a model of carrier transition from the shallow donor to the deep acceptor levels was established and studied [43]. Moreover, recent investigations have proposed that the YL emission in GaN films can be due to a $V_{\text{Ga}}\text{-O}_{\text{N}}$, single C_{N} defect, or $\text{C}_{\text{N}}\text{-O}_{\text{N}}$ compound [44–46]. Therefore, this information, coupled with the peak positions at 413 and 540 nm clearly observed in the low-temperature PL measurements, is useful for studying the defect states in GaN films to further improve the crystal quality.

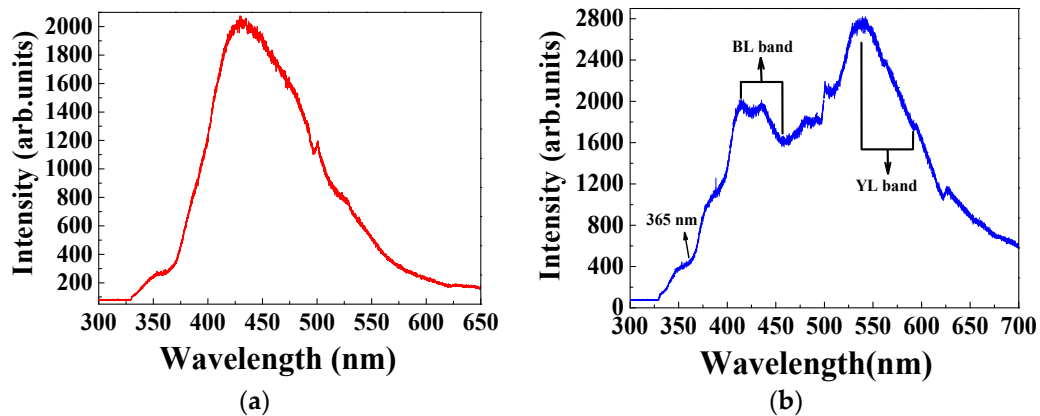


Figure 5. (a) Room temperature PL spectrum of GaN thin film with sputtering power of 75 W, and (b) the low-temperature PL spectra measured at 10 K.

The optical transmission spectra of the GaN films (Figure 6) showed that at sputtering powers of 75, 100, and 125 W, the average transmittance levels observed for the GaN films were 88.5%, 84.2%, and 81.6%, respectively, in the wavelength range of 400–1100 nm. The optical transmittance increased as the sputtering power decreased. The optical properties of the GaN films were determined to be significantly influenced by the difference in the average grain size and the surface morphology of a GaN film. The increase in optical transmittance as the sputtering power decreased could be attributed to an increase in grain size, as verified by the AFM measurement results. As the grain size increased, the reduced grain boundary scattering engendered an increase in optical transmittance [47].

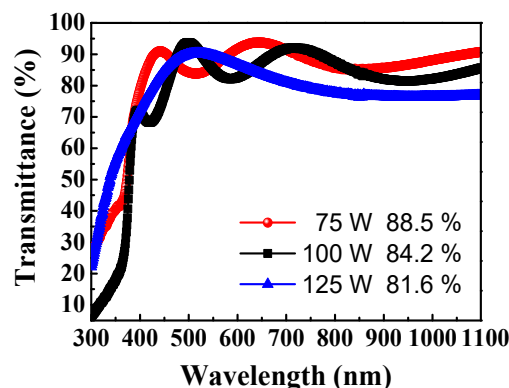


Figure 6. Optical transmittance of GaN thin films grown with different sputtering powers of 75, 100, and 125 W.

The observed optical transmittance was also significantly reduced in the wavelength range shorter than 375 nm, signifying that the absorption edge of the GaN film was at approximately 375 nm, which corresponded to an energy band gap of 3.4 eV, as verified by the PL results. Below the absorption edge

of 375 nm, discontinuities occurred in situations in which the energy of a high-energy photon was enough to excite electrons from the valence band to the conduction band; thus, the photon absorption phenomenon was dominant and led to the decrease in optical transmittance. Moreover, the light with an electromagnetic wave energy level lower than the GaN energy band gap was not absorbed but was rather transparent; thus, a high optical transmittance level was observed for the GaN films in the wavelength range longer than the absorption edge [48,49]. Therefore, in combination with the aforementioned arguments, the GaN film deposited at a power of 75 W had a high transmittance level along with a sharp absorption edge at approximately 375 nm because of its increased grain size, which is beneficial for high-performance optoelectronic applications.

However, a low nitrogen content was also observed for the GaN film. In this study, the GaN film was grown using a GaN target in a magnetron sputtering system with the argon and nitrogen gas as the process gases and the GaN thin films were grown at a low growth pressure and growth temperature, which indicated a low degree of nitrogen dissociation from the nitrogen process gas. Therefore, the low N content was observed in this study, and the modulation of nitrogen gas flow, growth temperature for the optimum growth condition is necessary for high quality GaN film growth.

4. Conclusions

This study investigated the sputtering deposition of high-quality GaN films with a ZnO buffer layer on an amorphous glass substrate by using pulsed DC sputtering. The experimental results show that the GaN film deposited at a sputtering power as low as 75 W and a low temperature of 300 °C exhibited improved columnar crystal growth and a polycrystalline structure.

At room temperature, PL measurement results reveal a typical NBE emission wavelength corresponding to a hexagonal GaN crystal structure at 365 nm with a deep defect level emission at 430 nm. Furthermore, low-temperature PL measurement results demonstrate that the defect emission peaks at 413 and 540 nm might have originated from a carrier transition through the C_{Ga} donor level to the C_N acceptor level and a YL emission in the GaN films, which was attributed to a $V_{Ga}-O_N$, single C_N defect, or C_N-O_N compound. From the observation of these defect levels in the PL measurements, GaN films possessing high crystal quality could be developed and grown through the reduction of deep defect levels. The XRD spectra of the GaN films revealed a *c*-axis (002) hexagonal wurtzite structure and a narrow FWHM value, with the predominant XRD peak being observed at a 2θ angle of approximately 34.5°. Additionally, the GaN film grown at a sputtering power of 75 W had a high transmittance level because of the large grain size obtained.

Considering the HRTEM results obtained for the ZnO buffer layer and GaN films, the lattice arrangement of the ZnO buffer layer was observed to be almost identical to that of a single-crystal ZnO film. In the HRTEM analysis of the GaN films, nanoisland structures with different orientations were noted, revealing a polycrystalline structure, but the lattice arrangement was nearly regular. From the SAED patterns of the GaN films, we can observe that the GaN film had a well-ordered SAED pattern of polycrystalline orientation spots. Moreover, the SIMS measurements were conducted on the GaN films to determine their chemical composition. The analyses of the GaN films and ZnO buffer layer indicated that they were chemically composed of Ga, N, Zn, C, and O elements. Therefore, the study results indicate that sputtering-deposited GaN films with a thin ZnO buffer layer on glass substrates can demonstrate a high crystal quality and have potential for fabrication and application in large-scale and low-cost GaN-related optoelectronic devices.

Author Contributions: Conceptualization, W.-S.L., Y.-L.C. and H.-Y.C.; Methodology, Y.-L.C. and H.-Y.C.; Validation, Y.-L.C. and H.-Y.C.; Formal Analysis, Y.-L.C. and H.-Y.C.; Investigation, W.-S.L.; Resources, W.-S.L.; Data Curation, Y.-L.C. and H.-Y.C.; Writing—Original Draft Preparation, Y.-L.C. and H.-Y.C.; Writing—Review and Editing, W.-S.L.; Visualization, W.-S.L.; Supervision, W.-S.L.; Project Administration, W.-S.L.; Funding Acquisition, W.-S.L.

Funding: This financial of this research was support under contracts MOST106-2221-E-155-041-MY3 by the Ministry of Science and Technology, Taiwan.

Acknowledgments: The authors are grateful to Jen-Inn Chyi at the National Central University for instrument support, and the Ministry of Science and Technology, Taiwan, R.O.C., for its financial support under contracts MOST106-2221-E-155-041-MY3. The provision of research equipment by the Optical Sciences Center and Center for Nano Science and Technology at National Central University is greatly appreciated.

Conflicts of Interest: The authors declare no conflict of interest.

References

- Jain, S.C.; Willander, M.; Narayan, J.; van Overstraeten, R. III-nitrides: Growth, characterization, and properties. *J. Appl. Phys.* **2000**, *87*, 965–1006. [[CrossRef](#)]
- Kumakura, K.; Makimoto, T. Carrier transport mechanisms of *Pnp* AlGaIn/GaN heterojunction bipolar transistors. *Appl. Phys. Lett.* **2008**, *92*, 093504. [[CrossRef](#)]
- Wang, X.L.; Wang, C.M.; Hu, G.X.; Wang, J.X.; Chen, T.S.; Jiao, G.; Li, J.P.; Zeng, Y.P.; Li, J.M. Improved DC and RF performance of AlGaIn/GaN HEMTs grown by MOCVD on sapphire substrates. *Solid-State Electron.* **2005**, *49*, 1387–1390. [[CrossRef](#)]
- Liu, L.; Edgar, J.H. Substrates for gallium nitride epitaxy. *Mater. Sci. Eng. R* **2002**, *37*, 61–127. [[CrossRef](#)]
- Tokunaga, H.; Tan, H.; Inaishi, Y.; Arai, T.; Yamaguchi, A.; Hidaka, J. Performance of multiwafer reactor GaN MOCVD system. *J. Crystal Growth* **2000**, *221*, 616–621. [[CrossRef](#)]
- Hughes, W.C.; Rowland, W.H., Jr.; Johnson, M.A.L.; Fujita, S.; Cook, J.W., Jr.; Schetzina, J.F. Molecular beam epitaxy growth and properties of GaN films on GaN/SiC substrates. *J. Vac. Sci. Technol. B* **1995**, *13*, 1571–1577. [[CrossRef](#)]
- Yu, H.; Chen, L.; Zhang, R.; Xiu, X.; Xie, Z.; Ye, Y.; Gu, S.; Shen, B.; Shi, Y.; Zheng, Y. The growth of GaN films on Si substrates by HVPE. *Mater. Sci. Forum* **2005**, *475–479*, 3783–3786. [[CrossRef](#)]
- Grandjean, N.; Massies, J.; Martinez, Y.; Vennegues, P.; Leroux, M.; Laugt, M. GaN epitaxial growth on sapphire (0 0 0 1): the role of the substrate nitridation. *J. Crystal Growth* **1997**, *178*, 220–228. [[CrossRef](#)]
- Zou, C.W.; Wang, H.J.; Yin, M.L.; Li, M.; Liu, C.S.; Guo, L.P.; Fu, D.J.; Kang, T.W. Preparation of GaN films on glass substrates by middle frequency magnetron sputtering. *J. Crystal Growth* **2009**, *311*, 223–227. [[CrossRef](#)]
- Zou, C.W.; Yin, M.L.; Li, M.; Liu, C.S.; Guo, L.P.; Fu, D.J. GaN films deposited on glass substrate by middle-frequency magnetron sputtering. *Thin Solid Films* **2008**, *517*, 670–673. [[CrossRef](#)]
- Sato, Y.; Kurosaki, A.; Sato, S. Low-temperature growth of GaN and In_xGa_{1-x}N films on glass substrates. *J. Crystal Growth* **1998**, *189/190*, 42–46. [[CrossRef](#)]
- Sellers, J. Asymmetric bipolar pulsed DC: the enabling technology for reactive PVD. *Surf. Coat. Technol.* **1998**, *98*, 1245–1250. [[CrossRef](#)]
- Kelly, P.J.; Arnell, R.D. Magnetron sputtering: A review of recent developments and applications. *Vacuum* **2000**, *56*, 159–172. [[CrossRef](#)]
- Schiller, S.; Goedicke, K.; Reschke, J.; Kirchhoff, V.; Schneider, S.; Milde, F. Pulsed magnetron sputter technology. *Surf. Coat. Technol.* **1993**, *61*, 331–337. [[CrossRef](#)]
- Barshilia, H.C.; Rajam, K.S. Reactive sputtering of hard nitride coatings using asymmetric-bipolar pulsed DC generator. *Surf. Coat. Technol.* **2006**, *201*, 1827–1835. [[CrossRef](#)]
- Hultman, L.; Helmersson, U.; Barnett, S.A.; Sundgren, J.E.; Greene, J.E. Low-energy ion irradiation during film growth for reducing defect densities in epitaxial TiN (100) films deposited by reactive-magnetron sputtering. *J. Appl. Phys.* **1987**, *61*, 552–555. [[CrossRef](#)]
- Jonsson, L.B.; Nyberg, T.; Katardjiev, I.; Berg, S. Frequency response in pulsed DC reactive sputtering processes. *Thin Solid Films* **2000**, *365*, 43–48. [[CrossRef](#)]
- Sun, X.W.; Xiao, R.F.; Kwok, H.S. Epitaxial growth of GaN thin film on sapphire with a thin ZnO buffer layer by liquid target pulsed laser deposition. *J. Appl. Phys.* **1998**, *84*, 5776–5779. [[CrossRef](#)]
- Xue, S.; Zhang, X.; Huang, R.; Zhuang, H. Effects of the sputtering time of ZnO buffer layer on the quality of GaN thin films. *Appl. Surf. Sci.* **2008**, *254*, 6766–6769. [[CrossRef](#)]
- Zou, C.W.; Zhanga, J.; Xie, W.; Shao, L.X.; Guo, L.P.; Fu, D.J. Characterization and properties of GaN films deposited by middle-frequency magnetron sputtering with anode-layer ion source assistance. *Vacuum* **2011**, *86*, 280–284. [[CrossRef](#)]
- Shi, F. GaN Nanowires Fabricated by Magnetron Sputtering Deposition. In *Nanowires—Fundamental Research*; Hashim, A.A., Ed.; InTech: London, UK, 2011; p. 265-262. ISBN 978-953-307-327-9.

22. Martínez-Ara, L.A.; Aguilar-Hernández, J.R.; Sastré-Hernández, J.; Hernández-Hernández, L.A.; Hernández-Pérez, M.d.; Maldonado-Altamirano, P.; Mendoza-Pérez, R.; Contreras-Puente, G. Structural and optical properties of GaN thin films grown on Si (111) by pulsed laser deposition. *Mater. Res.* **2019**, *22*, e20180263. [[CrossRef](#)]
23. Zhang, J.Z.L.D.; Wang, X.F.; Liang, C.H.; Peng, X.S.; Wang, Y.W. Fabrication and photoluminescence of ordered GaN nanowire arrays. *J. Chem. Phys.* **2001**, *115*, 5714–5717. [[CrossRef](#)]
24. Kim, K.H.; Park, K.C.; Ma, D.Y. Structural, electrical and optical properties of aluminum doped zinc oxide films prepared by radio frequency magnetron sputtering. *J. Appl. Phys.* **1997**, *81*, 7764–7772. [[CrossRef](#)]
25. Liu, W.-S.; Wu, S.-Y.; Tseng, C.-H.; Hung, C.-Y. Development of high-quality titanium-doped gallium ZnO transparent conductive films by RF magnetron sputtering techniques. *Phys. Status Solidi C* **2013**, *10*, 1569–1572. [[CrossRef](#)]
26. Liao, H.; Wei, T.; Zong, H.; Jiang, S.; Li, J.; Yang, Y.; Yu, G.; Wen, P.; lang, R.; Wang, W.; et al. Raman investigation on the surface carrier concentration of single GaN microrod grown by MOCVD. *Appl. Surf. Sci.* **2019**, *489*, 346–350. [[CrossRef](#)]
27. Kouvetakis, J.; Beach, D.B. Chemical vapor deposition of gallium nitride from diethylgallium azide. *Chem. Mater.* **1989**, *1*, 476–478. [[CrossRef](#)]
28. Bagavath, C.; Nasi, L.; Kumar, J. Investigations on the nanostructures of GaN, InN and In_xGa_{1-x}N. *Mater. Sci. Semicond. Process.* **2016**, *49*, 61–67. [[CrossRef](#)]
29. Ozgit-Akgun, C.; Kayaci, F.; Vempati, S.; Haider, A.; Celebioglu, A.; Goldenberg, E.; Kizir, S.; Uyar, T.; Biyikli, N. Fabrication of flexible polymer-GaN core-shell nanofibers by the combination of electrospinning and hollow cathode plasma-assisted atomic layer deposition. *J. Mater. Chem. C* **2015**, *3*, 5199–5206. [[CrossRef](#)]
30. Duygulu, N.E.; Kodolbas, A.O.; Ekerim, A. Effects of argon pressure and r.f. power on magnetron sputtered aluminum doped ZnO thin films. *J. Crystal Growth* **2014**, *394*, 116–125. [[CrossRef](#)]
31. Saad, M.; Kassis, A. Effect of rf power on the properties of rf magnetron sputtered ZnO: Al thin films. *Mater. Chem. Phys.* **2012**, *136*, 205–209. [[CrossRef](#)]
32. Jacob, D.; Chitra, M. Formation of GaN thin film on silicon substrate by gallium oxide Ammoniation. *Optik* **2018**, *171*, 51–57.
33. As, D.J.; Schmilgus, F.; Wang, C.; tker, B.S.; Schikora, D.; Lischka, K. The near band edge photoluminescence of cubic GaN epilayers. *Appl. Phys. Lett.* **1997**, *70*, 1311–1313. [[CrossRef](#)]
34. Schuberta, E.F.; Goepfert, I.D.; Grieshaber, W. Optical properties of Si-doped GaN. *Appl. Phys. Lett.* **1997**, *71*, 921–923. [[CrossRef](#)]
35. Reshchikov, M.A.; Morkoç, H. Luminescence properties of defects in GaN. *J. Appl. Phys.* **2005**, *97*, 061301. [[CrossRef](#)]
36. Reshchikov, M.A.; Shahedipour, F.; Korotkov, R.Y.; Ulmer, M.P.; Wessels, B.W. Deep acceptors in undoped GaN. *Phys. B* **1999**, *273–274*, 105–108. [[CrossRef](#)]
37. Reshchikov, M.A.; Shahedipour, F.; Korotkov, R.Y.; Wessels, B.W.; Ulmer, M.P. Photoluminescence band near 2.9 eV in undoped GaN epitaxial layers. *J. Appl. Phys.* **2000**, *87*, 3351–3354. [[CrossRef](#)]
38. Xue, S.; Zhang, X.; Huang, R.; Zhuang, H. Surface morphology of ZnO buffer layer and its effects on the growth of GaN films on Si substrates by magnetron sputtering. *Appl. Phys. A* **2009**, *94*, 287–291. [[CrossRef](#)]
39. Seager, C.H.; Wright, A.F.; Yu, J.; Gotz, W. Role of carbon in GaN. *J. Appl. Phys.* **2002**, *92*, 6553–6560. [[CrossRef](#)]
40. Seager, C.H.; Tallant, D.R.; Yub, J.; Gotz, W. Luminescence in GaN co-doped with carbon and silicon. *J. Luminesc.* **2004**, *106*, 115–124. [[CrossRef](#)]
41. Zhao, D.G.; Jiang, D.S.; Yang, H.; Zhu, J.J.; Liu, Z.S.; Zhang, S.M.; Liang, J.W.; Li, X.; Li, X.Y.; Gong, H.M. Role of edge dislocations in enhancing the yellow luminescence of n-type GaN. *Appl. Phys. Lett.* **2006**, *88*, 241917. [[CrossRef](#)]
42. Neugebauer, J.; van de Walle, C.G. Gallium vacancies and the yellow luminescence in GaN. *Appl. Phys. Lett.* **1996**, *69*, 503–505. [[CrossRef](#)]
43. Julkarnain, M.; Kamata, N.; Fukuda, T.; Arakawa, Y. Yellow luminescence band in undoped GaN revealed by two-wavelength excited photoluminescence. *Opt. Mater.* **2016**, *60*, 481–486. [[CrossRef](#)]
44. Ito, S.; Nakagita, T.; Sawaki, N.; Ahn, H.S.; Irie, M.; Hikosaka, T.; Honda, Y.; Yamaguchi, M.; Amano, H. Nature of yellow luminescence band in GaN grown on Si substrate. *Jpn. J. Appl. Phys.* **2014**, *53*, 11RC02. [[CrossRef](#)]

45. Reshchikov, M.A.; Demchenko, D.O.; Usikov, A.; Helava, H.; Makarov, Y. Carbon defects as sources of the green and yellow luminescence bands in undoped GaN. *Phys. Rev. B* **2014**, *90*, 235203. [[CrossRef](#)]
46. Christenson, S.G.; Xie, W.; Sun, Y.Y.; Zhang, S.B. Carbon as a source for yellow luminescence in GaN: Isolated CN defect or its complexes. *J. Appl. Phys.* **2015**, *118*, 135708. [[CrossRef](#)]
47. Yim, K.; Lee, C. Dependence of the electrical and optical properties of sputter-deposited ZnO: Ga films on the annealing temperature, time, and atmosphere. *J Mater. Sci.: Mater. Electron.* **2007**, *18*, 385–390.
48. Liu, W.-S.; Wu, S.-Y.; Hung, C.-Y.; Tseng, C.-H.; Chang, Y.-L. Improving the optoelectronic properties of gallium ZnO transparent conductive thin films through titanium doping. *J. Alloys Compd.* **2014**, *616*, 268–274. [[CrossRef](#)]
49. EKnox-Davies, C.; Shannon, J.M.; Silva, S.R.P. The properties and deposition process of GaN films grown by reactive sputtering at low temperatures. *J. Appl. Phys.* **2006**, *99*, 073503. [[CrossRef](#)]



© 2019 by the authors. Licensee MDPI, Basel, Switzerland. This article is an open access article distributed under the terms and conditions of the Creative Commons Attribution (CC BY) license (<http://creativecommons.org/licenses/by/4.0/>).